Chem

CellPress

Article

Scrolling of supramolecular lamellae in the hierarchical self-assembly of fibrous gels

Christopher D. Jones[1], Stuart R. Kennedy[1], Martin Walker[1], Dmitry S. Yufit[1] and Jonathan W. Steed[1,2]*

1. Department of Chemistry, Durham University, South Road, Durham, DH1 3LE, United Kingdom.
2. Lead contact
*Correspondence: jon.steed@durham.ac.uk

SUMMARY

Lamellar supramolecular assemblies are a common feature of fibrous gels formed by small molecules such as peptides and ureas. Competition between gelation and crystallisation is highly solvent-dependent, and may be governed by the dynamics of nascent lamellae in solution. We hypothesise that gel fibrils are formed when the scrolling of lamellae outpaces multilayer stacking. To test this model, extensive crystallographic data on model picolyl bis(urea)s were correlated with their gelation abilities. The majority of structures are lamellar, and gels involving fibrous aggregates form concomitantly alongside solvate structures. A distinguishing feature of these solvate crystals is that the lamellae are decorated with unequal numbers of picolyl groups on their upper and lower faces. Atomistic molecular dynamics (MD) simulations show that this asymmetry causes isolated lamellae to scroll spontaneously into fibrils, whereas symmetrical lamellae adopt flat, crumpled or saddle-like morphologies. Scrolling represents a general mechanism for gel formation, affording networks of unbranched fibres with monodisperse diameters dictated by the equilibrium curvature of the folding lamellae.

Keywords: Gel, supramolecular, hierarchical, lamellar, self-assembly, scrolling.

The Bigger Picture

Gels are extremely important soft materials with everyday applications in areas such as soaps, lubricants, catalysis and oilfield chemistry. While gels are commonly based on polymers, there is a great deal of interest in small molecule gelators that aggregate through non-covalent interactions such as hydrogen bonding and π-stacking to give 3D sample-spanning fibrous assemblies. The emergent complexity of gel structure is very difficult to predict and gelators are commonly discovered by trial and error. The properties of a gel depend on the structural evolution of its fibre network, but the mechanisms governing fibre growth are not currently understood. In this work we show that homogeneous gel fibres arise from the scrolling of sheet-like rafts of hydrogen bonded gelators whenever opposite sides of the sheet possess different surface energies. Based on this observation, we propose a general predictive mechanism for gel self-assembly.

INTRODUCTION

Low-molecular-weight gelators (LMWGs) are a varied and versatile family of molecules,[1] with potential applications in catalysis,[2] medicine[3] and crystal growth.[4] Increasing interest in LMWGs as alternatives to polymeric materials may be partly attributed to a growing understanding of their gelation mechanisms. Fibrous aggregation of an LMWG can be represented as a hierarchical process, beginning with the growth of one- or two-dimensional assemblies through supramolecular polymerisation (step 1). These assemblies develop into extended fibrils (step 2), which further entangle to generate the final gel network (step 3). By analogy with the levels of organisation in folded peptides,[5] the products of steps 1, 2 and 3 may be termed primary, secondary and tertiary structures respectively (Figure 1).[6] The primary structure of a gel describes the connectivity, symmetry and dimensionality of supramolecular motifs, and can often be reliably modelled on patterns of hydrogen bonding and stacking interactions in the gelator crystal structure(s).[7] However, it is more difficult to describe the architectures of secondary and tertiary structures at a molecular level. In particular, no general mechanism has been proposed to link the structure of a supramolecular

assembly to the morphology of the resulting aggregate. Addressing this deficiency would allow the gelation capacity of a molecule to be predicted based on its favoured supramolecular motifs, provide a robust theoretical foundation for analyses of gel aggregation, and facilitate the rational design of LMWGs to suit particular applications. Herein, we make use of insights from single-crystal diffraction and molecular dynamics (MD) simulations to develop a simple, predictive model of gel formation, wherein monolayers of gelator molecules scroll spontaneously into unbranched fibrils due to topological asymmetry in the hydrogen bonding network.

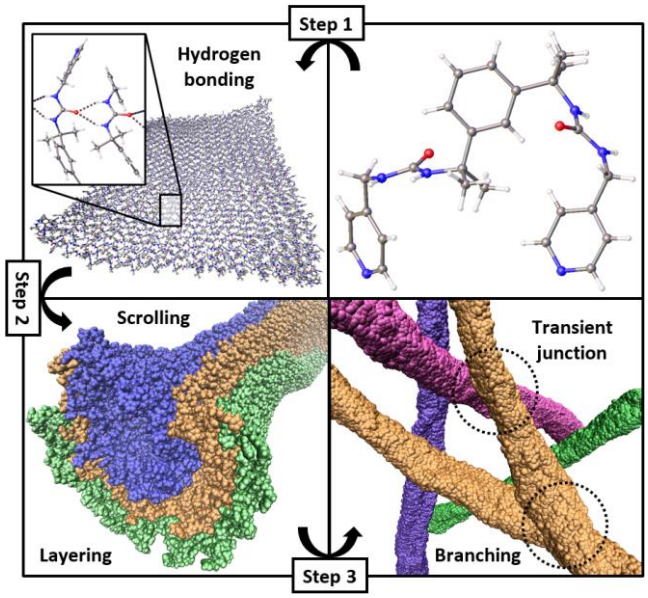

Figure 1 Stages in the hierarchical self-assembly of fibrous gels, according to the model proposed in this study. Small molecules self-assemble into lamellar structures (step 1), which subsequently give rise to cylindrical fibrils through scolling and layering (step 2). Fibrils undergo branching and entanglement to form a 3D network of larger fibres, which entrap solvent to produce a sample-spanning gel (step 3). Separate sheets and fibres are coloured differently for clarity.

With the aid of empirical structure-property relationships,[8] crystal engineering principles[9] and insights from spectroscopic and scattering experiments,[10-12] it is now possible to tune the physical properties of a wide variety of supramolecular gels. However, predicting the self-assembly behaviour of a potential LMWG *a priori* remains a challenge.[13] LMWGs can be designed in a modular fashion by incorporating functional groups known to give rise to fibrous assemblies, but the resulting gels may be affected in surprising ways by even small modifications to the gelator, solvent or preparation method. For example, gelation may depend on the enantiopurity of a chiral molecule,[14] the relative orientations of hydrogen bonding motifs,[15] the cooling rate of the gelling solution[16] or the properties of peripheral functional groups. Among gelators with an uneven balance of hydrogen bond donor and acceptor groups, the availability of water in an organic solvent is of particular importance due to the enhanced probability of hydrated solid forms.[17-20] Hydration may limit the potential for gel formation, by offering access to higher-symmetry packing modes with more optimal arrangements of hydrogen bonding motifs.[21]

Competition between gelation and crystallisation processes is a key feature of many LMWG systems. A gel often consists of microcrystals with a high aspect ratio,[22] and even non-crystalline gels may form alongside a non-gelating crystalline phase or undergo crystallisation with the passage of time.[23-25] Although the crystal structure of a gelator might offer some indication of how molecules interact in the gel phase,[26-28] the assumption of a structural relationship between the two materials is not always justified.[29,30] Nonetheless, it is likely that the dominant supramolecular motifs in crystals are preserved in the corresponding gels, and play a central role in determining the materials' optical, microstructural and rheological characteristics.[31] Indeed, Anderson *et al.* found that the calculated minimum-energy structures for hydrated melamine-uric acid co-crystals match the powder X-ray

diffraction patterns of the corresponding sonogels, and feature the most stable hydrogen bonding motifs identified through *ab initio* calculations.[28]

The likelihood of gelation is often strongly dependent on the solvent environment. Solvent molecules may co-assemble with an LMWG to produce aggregates with enhanced thermodynamic stability.[28,32] Additionally, solvation effects in the precursor sol may favour gelation by promoting self-assembly of the necessary supramolecular motifs. For example, carboxylic acid dimer synthons form more readily in the absence of competing hydrogen bonding species,[33] and the self-association of hydrophobic moieties may be strengthened by the use of a more polar solvent.[34] Owing to the large surface areas of nanoscale particles, a nascent gel aggregate may outcompete the nuclei of materials with higher bulk stability due to stabilising interactions with the surrounding solvent.[35] Similarly, solvation of growing surfaces may lead to large differences in their relative surface energies, producing the anisotropic growth conditions required for gel formation.[36]

To aid the identification of effective LMWGs, it is important to develop detailed computational models of the gelation process. Provided the system is well-parameterised and the force-field carefully chosen, MD simulations can replicate the key results of more realistic but computationally expensive calculation techniques. MD studies have been used to map the self-assembly pathways of peptides,[37-39] lipids[40,41] and polysaccharides,[42] as well as generalised polymers,[43-45] rod-shaped molecules[46,47] and colloidal particles.[48,49] Simulations have captured the formation of experimentally observable structures such as β-sheets, cylindrical micelles and phospholipid bilayers, and provided realistic illustrations of their interactions with solvents, ions and biologically relevant additives. As well as accurately reproducing measurable physical properties, such as critical gelator concentrations (CGCs), phase transition temperatures and packing coefficients, MD models have been used to probe less accessible parameters, including surface tensions, self-diffusion coefficients and molecular conformations.[40,50,51] Furthermore, some studies have yielded useful predictions. For instance, simulations of a triblock amphiphilic peptide highlight the potential for β-sheets to stack in a perpendicular fashion, producing soluble dimeric assemblies that could play an active role in neurological pathologies such as Alzheimer's disease.[37]

Lamellar structures are a common outcome in the self-assembly of hydrogen-bonding LMWGs. Crystalline materials arise when the stacking of lamellae occurs at a comparable rate to lateral growth, and may thus be favoured by high concentrations of nascent lamellae.[52] Gels, by contrast, are formed when disruption of long-range ordering results in extended fibrils and other anisotropic structures.[38,53-55] MD simulations of polymer sheets decorated with grafted tether coils indicate that curved morphologies are generated, in preference to multilayer stacks, when the upper and lower faces of the sheets are structurally dissimilar.[56-59] In general, fibril formation is attributed to hydrophobic effects, comparable to those observed in surfactant micelles.[60] For example, simulations of an amphiphilic alkyl dipeptide conjugate in water revealed the spontaneous self-assembly of cylindrical fibrils, with the extended alkyl residues encapsulated within the core of the aggregate.[38] Folding of lamellae may also be driven by the formation of hydrogen bonds or π-π stacking motifs, as contraction of the sheet on the convex face reduces the distance between interacting moieties.[56,61] The direction of folding and radius of curvature are dictated by the stiffness of the sheet[62] and the sizes and solvent affinities of the tether coils. While rigid sheets are unable to bend, those with smaller bending and tensile moduli may undergo both local and global deformation, producing crumpled, tubular and spheroidal morphologies.[63,64]

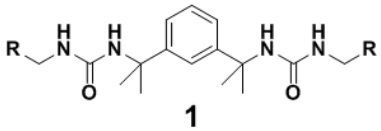

1

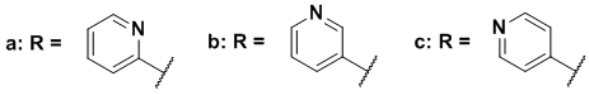

Modelling the development of lamellae into fibrous structures is a challenging task. Deformation of lamellae in solution may take place over tens or hundreds of nanoseconds, exceeding the timescales that can be easily probed in large-scale atomistic simulations. Moreover, model lamellae generated from randomly distributed gelator molecules are unlikely to reproduce all of the structural features affecting the aggregation pathway. A popular approach is to develop a coarse-grained representation of the system, identifying

molecular parameters that can be tuned to reproduce key physical characteristics.[65] Alternatively, the computational task may be simplified by comparing the simulated dynamics of pre-constructed, idealised aggregates.[61,66-70] Initial configurations may be justified based on the geometry of the LMWG, the relative energies of model assemblies, or the arrangements of molecules in single-crystal structures. By adopting an atomistic approach, and comparing the results for multiple lamellar systems, it is possible to test the impact of minor structural modifications and pinpoint the dominant contributions to the self-assembly outcome.

The aim of this investigation is to model key stages in the development of fibrous gels from hydrogen bonding LMWGs. In particular, we seek to explain why gel fibres are often unbranched and monodisperse, and how the formation of such structures can outcompete alternative crystallisation pathways. The focus of the study is a series of three isomeric bis(urea)s with picolyl end groups, **1a-c**. A number of experimental techniques, including small-angle neutron scattering,[71] powder X-ray diffraction[72] and scanning tunnelling microscopy,[70,73] have revealed lamellar structures in bis(urea) materials comparable to the β-sheets of peptide systems.[74] It is well documented that ureas self-assemble into continuous arrays of hydrogen bonds known as α-tape motifs,[75] which can readily give rise to anisotropic aggregates.[76] Simulations have been used to predict the morphologies and surface compositions of molecular clusters and demonstrate the influence of particular residues and supramolecular motifs on fibre propagation.[54,68] However, there have been few attempts to combine the results of atomistic simulations, single-crystal diffraction studies and coarse-grained models to provide a general and predictive description of gel formation.

An advantage of LMWGs comprising urea functionalities is their tendency to crystallise from a variety of organic solvents and exhibit many topologically distinct hydrogen bonding networks (Supplemental Information, Figures S26-36).[70,77-79] Compounds **1a-c** are of particular interest, as the limited flexibility of the sterically bulky spacer promotes the formation of unusual α-tape topologies.[80] Moreover, as in the extensively studied 3-pyridyl analogue,[81-83] the potential competition between hydrogen bond acceptors results in a diverse range of supramolecular outcomes. Although gels are formed only by **1c** in a small number of solvents, all of the compounds can access multiple lamellar crystal forms that may serve as starting points for simulating the aggregation process. We hypothesise that lamellar crystals are formed by stacking of preformed lamellae in solution, and aim to determine whether spontaneous deformation of such assemblies could lead to the concomitant fibrous aggregates experimentally observed. Examining a library of crystal structures offers insight into the influence of solvent on the molecular arrangement, and allows coarse structural features to be correlated with the presence or absence of a gel phase, highlighting useful trends that may facilitate the development of more effective LMWGs.

RESULTS AND DISCUSSION

Synthesis and structural characterisation

Compounds **1a-c** were synthesised by adding a diisocyanate to a chloroform solution of excess picolylamine (Supplemental Information, Figures S1-S12). The compounds were recrystallised from a range of polar solvents (Table 1) to produce single crystals of sufficient quality for analysis by single-crystal X-ray diffraction. In version 5.37 of the Cambridge Structural Database (CSD),[84] the majority of crystal structures comprising bis(urea)s linked by α-tape motifs consist of one-dimensional hydrogen bonded supramolecular polymers (Tables S3 and S4). However, nearly all the structures in this study consist of layers of molecules linked by two-dimensional networks of α-tapes. This pattern of motifs is likely favoured in order to minimise steric clashes between the bulky spacer moieties of neighbouring molecules. Similarly, it is sometimes preferable for the achiral molecules to crystallise in chiral space groups or exhibit one or more polar axes, corresponding to a common orientation of the urea moieties or a head-to-tail arrangement of asymmetric lamellae.

Bis(urea)s may form supramolecular polymers with a wide variety of conformations,[85] but the network of α-tapes will typically conform to a common pattern of connectivity. The topologies of the bis(urea) networks are categorised by assigning a common letter to molecules sharing a pair of tapes (Figure 2). For example, bis(urea)s adopting a “brick wall” arrangement are tape-sharing with molecules in alternating rows, so the repeat unit of each α-tape is denoted [AB]. All lamellar bis(urea) crystal structures so far reported display one of just two network topologies: [AB] and [AABB] (Tables S3 and S4). However, the suitability of lamellae for gel formation also depends on their symmetry and morphology, which may be strongly perturbed by changes to the molecular structure or solvent environment. Although

the crystal structures of compounds **1a-c** generally consist of lamellae with similar supramolecular motifs, altering the configuration of the picolyl group can greatly affect the interlayer interactions and favourability of solvate formation.

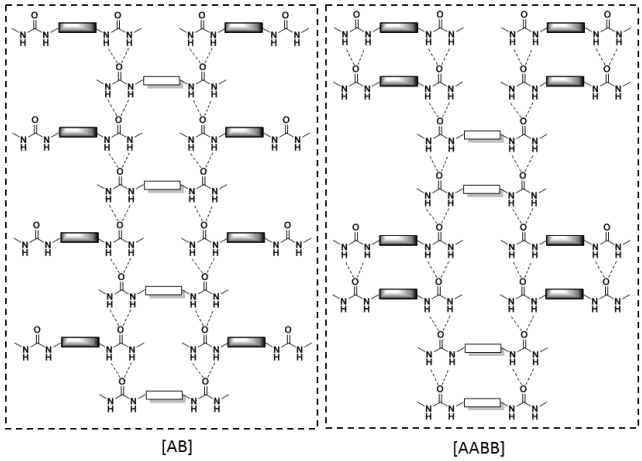

Figure 2 The two most common topologies of lamellar α-tape networks. Within each α-tape, molecules are labelled with a common letter if they are also connected via a second α-tape. These "tape-sharing" bis(urea)s are represented schematically as white (A) or black (B) spacers linking two urea moieties, with dashed lines indicating hydrogen bonds.

Non-solvated assemblies

In their non-solvated crystal structures, compounds **1a** and **1b** both display an [AB] packing arrangement. However, the morphologies of the lamellar networks differ due to the variable ability of picolyl groups to form hydrogen bonds. In crystals of **1a** (structure **I**, Table 1) obtained by recrystallisation of **1a** from nitromethane or 3-picoline, the spacer of the bis(urea) is nearly parallel to the lamellar plane. Thus, lamellae are relatively thin, with an interlayer spacing d_{layer} of 7.553(1) Å and lamellar area A_{mol} of 83.55(2) Å^2 per molecule. This packing mode is favoured because the bis(urea)s do not form the common $R_2^1(6)$ urea-urea motifs,[86] but instead interact via single urea-urea and picolyl-urea hydrogen bonds (Figure 3). The resulting $R_2^1(11)$ motifs force the picolyl and urea groups to lie in approximately the same plane, with no significant interactions between neighbouring lamellae. Such an arrangement of hydrogen bonds is not possible in crystals of **1b** and **1c**, as it is not geometrically feasible for the nitrogen atoms of 3- and 4-picolyl groups to approach the hydrogen bond donors of adjacent urea-urea motifs.

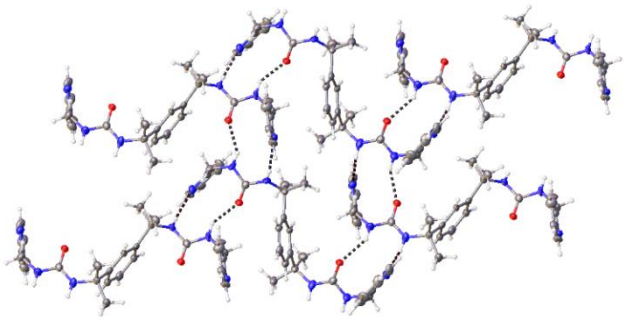

Figure 3 Lamellar hydrogen bonding network in structure **I**, viewing down the normal axis of the lamellar plane. Molecules of **1a** are linked by urea-urea and picolyl-urea interactions (dashed lines).

Table 1. Summary of crystallographic data

	1a (I)	**1b (II)**	**1b (III)**	**1b**·2H_2O (**IV**)	**1c**·(C_6H_7N) (**V**)	**1c**·0.5(C_6H_7N) (**VI**)
Formula	$C_{26}H_{32}N_6O_2$	$C_{26}H_{32}N_6O_2$	$C_{26}H_{32}N_6O_2$	$C_{26}H_{36}N_6O_4$	$C_{32}H_{39}N_7O_2$	$C_{58}H_{71}N_{13}O_4$
Formula weight	460.57	460.57	460.57	496.61	553.70	1014.27
Space group	$P2_1$	$P2_12_12_1$	*Pbca*	$P2_1/c$	$P2_1$	*P*-1
***a* / Å**	11.1606(17)	9.3865(12)	12.1736(15)	20.9540(16)	9.2277(6)	15.1050(18)
***b* / Å**	9.0613(14)	11.4758(14)	9.2491(12)	15.2334(12)	11.2568(7)	18.340(2)
***c* / Å**	12.6316(19)	23.407(3)	43.427(5)	18.0568(14)	15.1469(9)	20.543(2)
α / °	90	90	90	90	90	88.283(3)
β / °	101.436(5)	90	90	110.150(3)	105.978(2)	76.761(3)
γ / °	90	90	90	90	90	89.450(3)
***V* / Å^3**	1252.1(3)	2521.3(5)	4889.7(10)	5411.0(7)	1512.59(16)	5537.1(11)
Z	2	4	8	8	2	4
***D*$_{calc}$ / g cm^{-3}**	1.222	1.213	1.251	1.219	1.216	1.217
***R*$_{int}$**	0.0711	0.1270	0.1571	0.1615	0.0690	0.1020
***R*$_1$ [*I* ≥ 2σ (*I*)]**	0.0615	0.0533	0.0881	0.1202	0.0487	0.0848
***wR*$_2$ [all data]**	0.1660	0.1150	0.1960	0.3240	0.1098	0.2147

	1c·0.5(C_6H_7N) (**VII**)	**1a**·0.5$PhNO_2$·0.25H_2O (**VIII**)	**1c**·1.25$PhNO_2$·0.25H_2O (**IX**)	**1c**·2$MeNO_2$ (**X**)	**1c**·2MeCN (**XI**)
Formula	$C_{58}H_{71}N_{13}O_4$	$C_{116}H_{140}N_{26}O_{13}$	$C_{134}H_{155}N_{29}O_{19}$	$C_{28}H_{38}N_8O_6$	$C_{28}H_{38}N_8O_6$
Formula weight	1014.27	2106.53	412.64	582.66	542.68
Space group	*I*2/*a*	$P2_1/c$	*P*-1	*Fdd*2	*Fdd*2
***a* / Å**	16.000(14)	15.2876(11)	15.6876(10)	29.2830(14)	28.9722(16)
***b* / Å**	36.172(3)	35.975(3)	18.4655(12)	34.2175(16)	34.2485(19)
***c* / Å**	20.309(2)	20.6493(15)	22.7146(14)	12.0618(6)	12.1561(7)
α / °	90	90	82.8733(19)	90	90
β / °	106.865(4)	103.288(3)	87.1357(18)	90	90
γ / °	90	90	83.168(2)	90	90
***V* / Å^3**	11248.6(18)	11052.4(14)	6478.6(7)	12085.8(10)	12061.9(12)
Z	8	4	2	16	16
***D*$_{calc}$ / g cm^{-3}**	1.198	1.266	1.269	1.281	1.195
***R*$_{int}$**	0.0876	0.0898	0.1135	0.0597	0.0636
***R*$_1$ [*I* ≥ 2σ (*I*)]**	0.0665	0.0587	0.0935	0.0676	0.0426
***wR*$_2$ [all data]**	0.1983	0.1367	0.2904	0.1777	0.0927

The geometry of a bis(urea) lamella may also be influenced by the symmetry of the α-tape network. In the non-solvated crystal forms of **1b (**structures **II** and **III**, Table 1**)**, the configurations of α-tapes are markedly different. Structure **II** was crystallised from an acetonitrile solution and comprises α-tapes in the relatively common antiparallel arrangement (Figure 4a). There are no other significant supramolecular motifs within each lamellar bis(urea) network. However, pairs of lamellae are linked by bifurcated urea-urea-picolyl hydrogen bonds, which lead to pronounced asymmetry in the $R_2^1(6)$ urea-urea motifs. Since molecules are not constrained to lie in the plane of the α-tape network, the bis(urea) assemblies are thicker than those in structure **I** and more highly interdigitated, with d_{layer} = 11.704(2) Å and A_{mol} = 53.86(1) Å^2.

A second polymorph of **1b** (structure **III**) was crystallised from nitrobenzene. Owing perhaps to competitive solvent-urea hydrogen bonding during the self-assembly process, the material does not exhibit any significant picolyl-urea interactions. In addition, the structure consists of polar α-tape networks, in which all interconnected urea groups exhibit the same orientation (Figure 4b). It has been suggested that syn-parallel tapes are less favourable than antiparallel networks as a result of destabilising dipole interactions between neighbouring ureas.[87] However, examination of bis(urea) crystal structures in the CSD[88] (Table S2) reveals that around 40% of bis(urea)s with urea-urea interactions exhibit a parallel intramolecular arrangement of urea groups (Table S3). Indeed, while structure **III** lacks the additional interlamellar hydrogen bonding of structure **II**, its density is 3% higher due to more efficient interdigitation of neighbouring lamellae (d_{layer} = 10.857(2) Å, A_{mol} = 56.30(1) Å^2). It appears that each polymorph of **1b** represents a different compromise, providing a stable balance

between the competing demands of picolyl-urea hydrogen bonding and crystal packing efficiency.

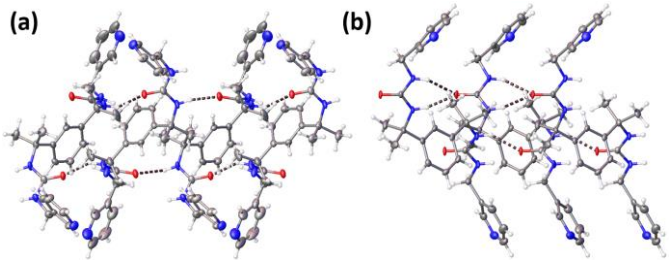

Figure 4 Lamellar networks in the non-solvated polymorphs of **1b**, viewing along the lamellar planes and perpendicular to the α-tapes. Adjacent α-tapes are antiparallel in structure **II** (a) and syn-parallel in structure **III** (b).

Solvated assemblies

By crystallising as solvates, compounds **1a-c** can acquire a more balanced ratio of hydrogen bond donors to acceptors.[89] Recrystallisation of **1b** from wet methanol produced a dihydrate (structure **IV**), which displays an [AABB] network of α-tapes. The water molecules form a linear trimer, and bridge adjacent lamellae via one urea-water and two picolyl-water hydrogen bonding motifs (Figure 5).

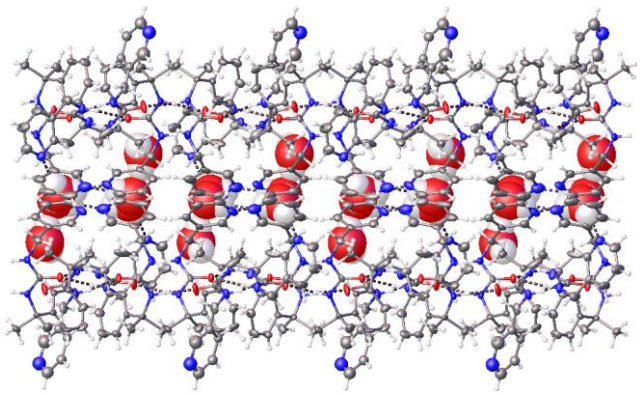

Figure 5 A pair of lamellar networks in the dihydrate of **1b**, structure **IV**, viewing along the lamellar planes and perpendicular to the α-tapes. Hydrogen-bonded water trimers (shown in space-filling representation) link pairs of lamellae via interactions with the pendant picolyl groups. Disorder in the picolyl groups and the fourth water molecule in the asymmetric unit are omitted for clarity.

Solvate formation by compounds **1a-c** is not restricted to solvents that are strong hydrogen bond donors. Indeed, compound **1c** forms crystalline solvates with both 3- and 4-picoline, guests that are unable to engage in strong hydrogen bonding with the picolyl end groups. The 4-picoline solvate (structure **V**) consists of an [AB] α-tape network. One NH group in half of the urea groups forms a hydrogen bond with the picoline guest molecule (Figure 6a), but the picolyl end groups of the bis(urea) are not involved in any significant supramolecular motifs. By contrast, crystallisation of **1c** from 3-picoline affords two concomitant polymorphic solvates that both exhibit interacting picolyl moieties. In structure **VI**, [AABB] bis(urea) lamellae are arranged as bilayers linked by picolyl-picolyl π-π stacking motifs (Figure 6b). In structure **VII**, bis(urea) molecules are organised into an unprecedented [AAAABBBB] network, and there is one example each of picolyl-urea and solvent-urea hydrogen bonding (Figure 6c).

Optimisation of hydrogen bonding and crystal close packing is sometimes best achieved through the formation of a ternary crystal structure. Nitrobenzene solvates of **1a** and **1c** (structures **VIII** and **IX** respectively) may be crystallised from wet nitrobenzene, and both systems incorporate molecules of water alongside the main crystallisation solvent. The two

structures both comprise lamellar bis(urea) networks bridged by picolyl-water hydrogen bonds. Furthermore, the asymmetric units of both structures are unusually large: in addition to four bis(urea) molecules and one molecule of water, there are two symmetry-independent nitrobenzene molecules in structure **VIII** and five in structure **IX**. Despite these similarities, the molecular arrangements of the crystals are starkly different. Tape networks in structure **VIII** exhibit an [AAAABBBB] topology, and the faces of the lamellae are symmetry equivalent, even though the picolyl groups of each bis(urea) molecule are oriented in the same direction (Figure 7a). Lamellae in structure **IX**, meanwhile, consist of [AABB] repeat units, in which half of the tape motifs are fragmented into discrete tetramers of interacting ureas (Figure 7b). The missing urea-urea hydrogen bonds are replaced with picolyl-urea interactions which, due to the asymmetric arrangement of bis(urea) molecules, are confined to one side of the lamellar network. Likewise, most of the bis(urea) molecules adopt a roughly C-shaped conformation, such that one face of the lamella accommodates three quarters of the picolyl end groups.

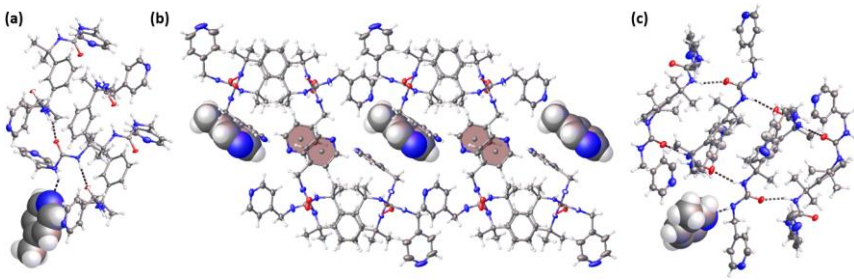

Figure 6 Major supramolecular motifs in the picoline solvates of **1c**: (a) hydrogen bonding between 4-picoline and a urea group in structure **V** (N-N distance 3.200(4) Å); (b) solvent-picolyl and picolyl-picolyl π-π stacking in structure **VI** (centroid separations 3.848(2) and 3.799(4) Å and plane-to-plane angles of 8.95(13) and 0.0° respectively); (c) hydrogen bonding between 3-picoline and a urea group in structure **VII** (N-N bond distance 3.1330(2) Å), showing the unusual subunit of four tape-sharing molecules. Solvent is shown in a space-filling representation and the centroids and mean planes of π-π stacked rings are marked. Additional solvent molecules in structures **VI** and **VII** and the extensive disorder in structure VII are omitted for clarity.

Fragmentation of α-tape motifs generates "free" NH and carbonyl groups that can interact with bis(urea)s in adjacent tape networks. In structure **IX**, matching faces of neighbouring lamellae are linked by bifurcated picolyl-urea-picolyl hydrogen bond motifs. It is evident, however, that an alternative polar (head-to-tail) stacking of lamellae would allow for the formation of additional urea-urea hydrogen bonds. Arrangements of this type are observed in the isostructural nitromethane and acetonitrile solvates of **1c** (structures **X** and **XI** respectively). The structures may be viewed as stacks of [AABB] lamellae in which half of the α-tapes have been fragmented, allowing the urea groups to interact with those of neighbouring lamellae to produce a three-dimensional network (Figure 7c). Every bis(urea) molecule forms a pair of urea-urea motifs with one of its neighbours. However, no two non-adjacent molecules are tape-sharing, because the tapes formed by each bis(urea) are aligned with different diagonals of the (100) plane. To the best of our knowledge, non-parallel α-tapes have never been observed in a bis(urea) system and are almost unprecedented among related compound classes. Indeed, an extensive search of the CSD reveals just one other structure in which α-tapes adopt a non- parallel arrangement: form II of tolbutamide (CSD refcode ZZZPUS05), a highly polymorphic mono(urea) used in hypoglycemia treatment.[90]

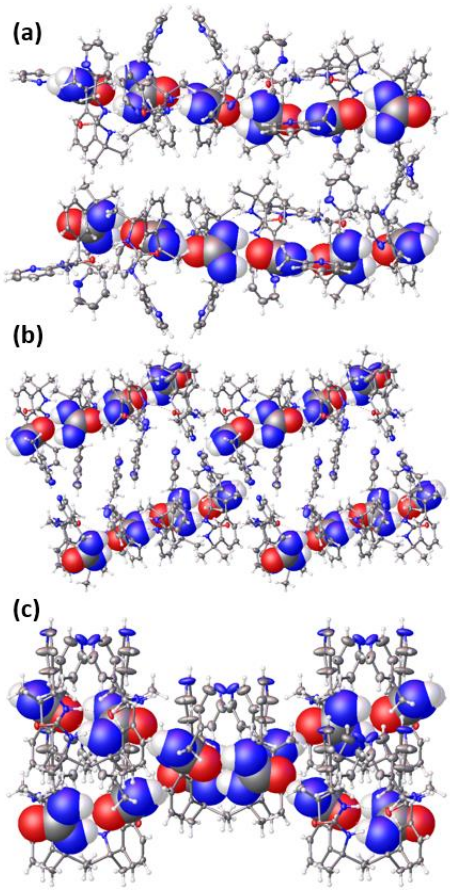

Figure 7 Varying orientations of α-tapes, viewing down a: (a) antiparallel α-tapes in two lamellae of structure **VIII**; (b) fragmented tape motifs in two lamellae of structure **IX**; (c) non-parallel α-tapes in structure **X**. For clarity, solvent is omitted and only half of the urea groups are shown in space-filling representation.

Structures **X** and **XI** are the only examples of three-dimensional hydrogen bonded networks in this study. In structures **I**-**IX**, lamellae may be categorised according to the presence of asymmetry between the upper and lower faces. While bis(urea) networks in structure **IX** are the most dramatically asymmetric, structure **VII** also displays an uneven packing arrangement: half of the picolyl groups on one lamellar face lie roughly parallel to the lamella, while all of those on the opposite side adopt an extended conformation. Similarly, structure **III** contains two symmetry-independent α-tapes, which occur on different sides of the lamellar plane. In all other systems, the faces of lamellae are symmetry equivalent. It is hypothesised that the symmetries of the crystalline systems are shared by the solution-phase lamellae from which they develop. As in micellar assemblies,[60] asymmetric features may promote high-curvature aggregate morphologies, causing fibrous structures to be favoured over crystalline materials under certain self-assembly conditions.

Gelation *vs* crystallisation

Gels of small molecules are typically prepared by cooling a solution of the gelator beyond the point of saturation. Although compounds **1a** and **1b** dissolve readily in a number of solvents upon heating, cooling or evaporation of the solutions produces crystalline precipitates and not gels. By contrast, boiling a nitrobenzene solution of **1c** in a sealed vial and allowing the solution to cool to room temperature produces a gel if the concentration exceeds the critical gelator concentration (CGC) of 0.5% (w/v) (Figure S15). Gelation of 1% (w/v) solutions typically occurs over 10-20 minutes, whereas 0.5% (w/v) solutions form weak or partial gels over 1-2 hours. Crystals of the hydrated nitrobenzene solvate **IX** occur concomitantly within the gels and are usually small and polycrystalline in nature. Crystallisation is relatively slow and leads to a marked increase in opacity as the gel is left to stand.

The microstructures of the nitrobenzene gels of **1c** were examined by scanning electron microscopy (SEM). SEM images of the platinum-coated xerogels reveal a network of unbranched fibres and entrapped rod- and plate-shaped microcrystals (Figures 8a, 8b and S19). The diameters of the fibres are variable with a maximum value in the region of 60 nm. The majority of fibres consist of approximately monodisperse fibrils 20 nm in thickness. Given that a small fraction of fibres are thicker and more crystalline in appearance, it is possible that aggregation of the bis(urea) affords a variety of assemblies, diverging from the lamellar crystal structure in a continuous fashion.[27] A fibrous material can also be obtained from nitromethane alongside octahedral single crystals (Figures 8c, 8d and S16). The nitromethane solvate of **1c**, structure **X**, displays a more isotropic habit than the nitrobenzene solvate due to the presence of a three-dimensional network of α-tapes. Likewise, the fibres in this system are shorter and less abundant, and coalesce into a gelatinous precipitate of isolated clusters rather than a sample-spanning gel.

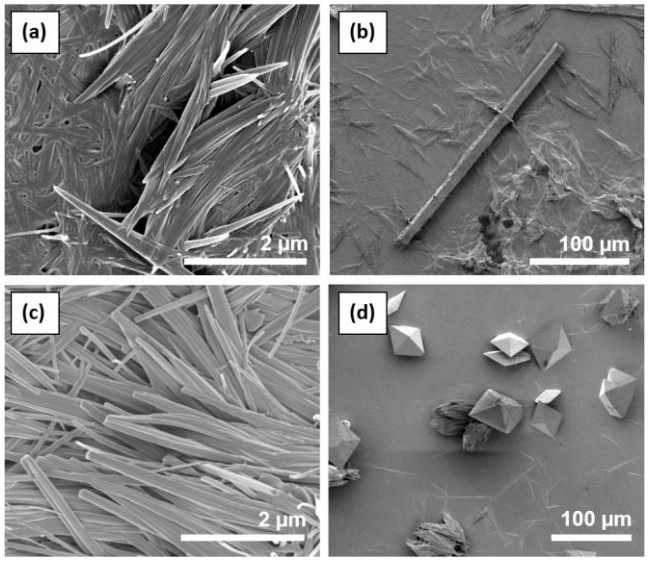

Figure 8 SEM micrographs of platinum-coated xerogels prepared from 1% (w/v) gels of **1c**. Fibres in the nitrobenzene gel (a) entrap rod-shaped crystals of solvate **IX** (b). Fibres in the nitromethane partial gel are shorter but of similar diameter (c), while concomitant crystals of the **1c** nitromethane solvate **X** exhibit an octahedral habit (d).

The rheological properties of the nitrobenzene gel of **1c** were characterised by oscillatory shear rheometry. The stress-strain profile of a 2% (w/v) gel at an oscillation frequency $\omega = 1$ Hz reveals the expected viscoelastic behaviour at low shear stresses, marked by a storage modulus G' one order of magnitude larger than the loss modulus G'' (Figure 9). The material exhibits an initial G' value of 21-25 kPa and undergoes liquefaction at a yield stress of approximately 240 Pa, which are typical values for a moderately rigid small-molecule gel. The frequency response of the material is also characteristic of a true gel: G' is almost independent of ω, as predicted by the soft glassy rheological (SGR) model of shear deformation (Figures S13a and S13b).[91]

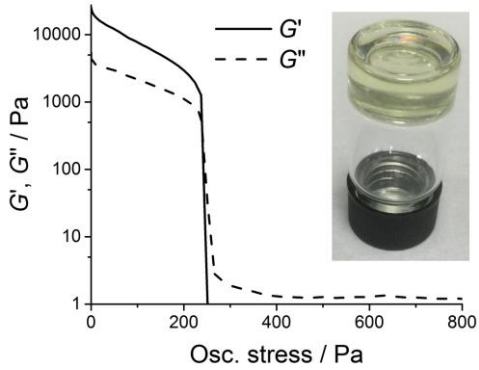

Figure 9 Oscillatory stress sweep profile of a 2% (w/v) gel of **1c** in nitrobenzene. The gel passes the inversion test (inset) but collapses spontaneously on standing, perhaps due to ongoing crystallisation.

It is not clear to what extent the structure of the gel fibres resembles that of the hydrated nitrobenzene solvate of **1c**, structure **IX**. The powder X-ray diffraction pattern of a dried 1% (w/v) gel reveals sharp reflections attributable to a crystalline phase, but poorly matches the calculated pattern of structure **IX** (Figure S14). It is possible that the microcrystals observed alongside single crystals of structure **IX** correspond to alternative solvate structures, or that additional crystalline phases are formed by desolvation or recrystallisation when drying takes place. Neither the dried or wet gels display broad reflections with the characteristic distribution of a lamellar aggregate.[69] However, it is noted that gel fibrils are only 2-4 times wider than the interlayer spacing in structure **IX**, so the presence of locally ordered layers is unlikely to give rise to a clear diffraction pattern. Given that lamellae are observed in the vast majority of crystals formed by **1c**, it is reasonable to assume that molecules in the gel are also incorporated into lamellar assemblies. Indeed, neutron scattering data for similar gels under thin-film shearing are consistent with a lamellar structure, and confirm that the *d*-spacings of the lamellae and radii of the gel fibres are comparable in magnitude.[71]

Structure **IX** is a hydrated system, in which water contributes hydrogen bonds to bridge the picolyl groups of neighbouring lamellae. Given that hydration is expected to favour multilayer assemblies by strengthening interlamellar interactions, the competition between gelation and crystallisation in this system is likely to be influenced by the availability of water. Systematic testing reveals that a 1% (w/v) solution of **1c** can only undergo gelation at water concentrations less than 0.3% (w/v). This threshold scales roughly linearly with the quantity of gelator, reaching values of 0.5 and 0.7% (w/v) respectively for gelator concentrations of 2 and 3% (w/v). Thus, it can be deduced that inhibiting gel formation requires around six water molecules per molecule of gelator, corresponding to 25 times the quantity that may be incorporated into crystals. Precipitates above the CGC of the gelator tend to consist of small plates or polycrystalline materials, regardless of whether gelation takes place. In a 0.2% (w/v) solution, however, the presence of up to 1% (w/v) of water typically results in large plates suitable for analysis by single-crystal X-ray diffraction. Higher water concentrations cause the size and quality of crystals to be markedly reduced, while concentrations significantly below 0.2% (w/v) do not induce observable precipitation (Figures S17 and S18).

Nitrobenzene gels of **1c** are metastable under ambient conditions and, in 2 cm^3 vials, tend to collapse over several days. Intriguingly, however, this process is greatly accelerated if the gel is prepared in a larger vial. In other small-molecule systems, relationships between aggregation outcome and container size have been linked to variations in nucleation rate and fibre density.[92] To monitor this effect in a quantitative fashion, 3 cm^3 of a 1% (w/v) solution were added directly to a mould on the geometry stage at 20ºC, and subjected to a shear stress of 1 Pa with ω = 1 Hz. G' increased for approximately 10 minutes but decreased spontaneously thereafter, suggesting that disruption of the gel coincides with the increased precipitation of crystalline material (Figure S13c). Notably, the gel may be regenerated after collapse via heating-cooling cycles in a sealed vial. Thus, destabilisation of the gel is not attributable to the gradual uptake of environmental water, as this would lead to a permanent loss of gelation behaviour.

Lamellar self-assembly

A requirement for the formation of fibrous gels is that self-assembly occur preferentially in one or two directions. Lamellar networks of bis(urea)s are likely to adopt this mode of aggregation, as crystal growth generates new urea-urea motifs only if it occurs parallel to the lamellar plane. One way to quantify this anisotropy is to perform MD simulations of differently sized crystallites and assess how the inclusion of additional layers of molecules affects the energy of the system. It is noted that the majority of crystal structures display similar urea-urea hydrogen bonding synthons and only weak interactions between neighbouring lamellae. Thus, identifying favoured growth axes in one such system would strongly support the possibility of isolated lamellar assemblies, which can expand into large-scale anisotropic aggregates rather than stacking to produce a multilayer crystallite.

To probe the behaviour of bis(urea) assemblies in the absence of solvent, and minimise the time required for equilibration of the system, atomistic MD simulations were performed in a vacuum under constant-*NVT* conditions. Crystallites of between 1200 and 3600 molecules were simulated in GROMACS 4.6.2[93] using the General Amber Force Field (GAFF),[94] with charges and interaction parameters assigned via the Antechamber package.[95] The initial structures were obtained from single-crystal data, bounded with a 50 nm cubic periodic box and subjected to an initial energy minimisation step via a steepest-descent procedure. Production runs were performed using a 1 fs time step, with random initial velocities assigned according to a Maxwell distribution at 300 K. The temperature was controlled via a Berendsen thermostat with a time constant of 0.1 ps.[96] Although it fails to generate a correct canonical ensemble, the Berendsen thermostat was chosen as it effects efficient convergence of both temperature and potential energy, allowing the dynamics of many systems to be compared under isothermal conditions over extended timescales (Figure S22a).

For each model crystallite, an initial equilibration was performed over 150 ps under constant-*NVT* conditions. The simulation was then continued for an additional 150 ps, recording the potential energy of the system at 5 ps intervals. A short time period was allocated for the analysis as energies were found to converge rapidly under the simulation conditions. The mean potential energy over the final 150 ps period was equated to the equilibrium energy of the crystallite, E_{tot}. The energy of each crystal face, E_{face}, was estimated by measuring the change in E_{tot} upon varying the number of unit cells along the face normal axis. In a crystallite of N layers, there are (N–1) interfaces between layers. Thus, the value of E_{face} may be calculated from the gradient of the straight line obtained by plotting E_{tot}/N against $1/N$ (Figure 10). The remaining energy in each layer, E_{bulk}, comprises the internal energy of the bulk lattice and surface energies of the edge faces, and largely determines the intercept value.

$$\frac{E_{\mathrm{tot}}}{N} = \frac{-E_{\mathrm{face}}}{N} + (E_{\mathrm{bulk}} + E_{\mathrm{face}}) \qquad (1)$$

To obtain a measure of the surface energy, γ, E_{face} must be divided by twice the area of the crystal face, since increasing N by one removes a free surface from both the original crystallite and the additional layer. It is possible that such values could be estimated more quickly by subtracting the energy of the simulated crystal bulk from that of a surface slab.[35,36] An advantage of the approach used in this study is that increasing N resembles the actual process of aggregation. Furthermore, the discrete crystallites are closer analogues to real assemblies than an infinite periodic lattice, and the calculation of a gradient through multiple points allows the precision of γ to be easily assessed.

It is relatively difficult to obtain reliable estimates of γ for crystallites containing loosely bound solvent, or for pairs of parallel crystal faces that are not symmetry equivalent. For simplicity, therefore, γ values were estimated for structure **II**, which consists of non-solvated lamellae with no polar axes. Although the molecules in this structure show no gelation capability, they exhibit supramolecular motifs comparable to those of structure **IX**. This structure, in turn, crystallises concomitantly with nitrobenzene gels of **1c**, and thus serves as the best available model for the gel fibril structure. Four data points were obtained for each lattice vector, and E_{tot} was calculated as the average energy of 100 points spanning 150 ps, with a step size of 1 fs and 150 ps of equilibration time (Figure S20).

The potential for anisotropic growth may be gauged from the relative magnitudes of γ parallel and perpendicular to the plane of the lamella. Along (100) and (010), the vectors parallel to the α-tape network, γ values of 124 ± 1 and 114 ± 2 mJ m^{-2} were obtained. The similarity in these values is unsurprising given that layers of molecules along both lattice vectors interact via strong urea-urea hydrogen bonds. By contrast, the lamellar plane itself is decorated with picolyl moieties, and half of these form picolyl-urea hydrogen bonds with neighbouring lamellae. The corresponding γ value, 88 ± 1 mJ m^{-2}, is 23-29% smaller than the values for the

other crystal faces. These results support the hypothesis that self-assembly in the absence of strong solvent-gelator interactions can produce isolated monolayers well suited to gel formation. More polar solvents may give rise to crystallisation, or the concomitant formation of crystals and gels, because surface solvent-urea interactions produce more isotropic γ values and a stronger tendency for three-dimensional self-assembly. Nonetheless, it is possible from estimates of γ in a vacuum to correctly predict the smallest and largest faces of the plate-shaped crystals, which correspond to the (001) and (100) planes respectively of the bis(urea) lamellae (Figure S21).

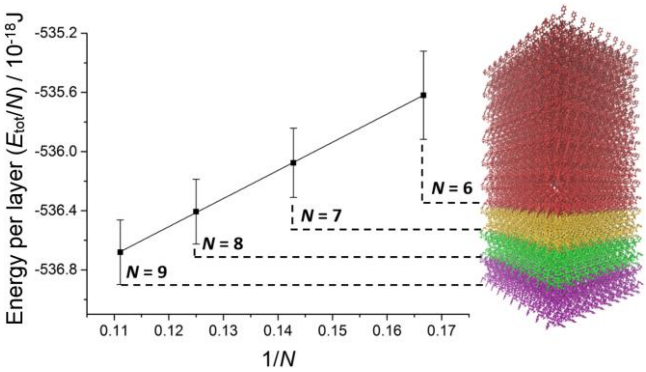

Figure 10 Plot to determine surface energy γ of the lamellar (001) plane in structure **II**. Error bars indicate the standard deviation of the energy values over the final 150 ps of each 300 ps simulation. The linear trend line was fitted by least-squares analysis and exhibits an R^2 of 0.9998, with an error in the gradient of 0.004%. The smallest model crystallite, shown in red, consists of 6 lamellae with 400 molecules per lamella. Illustrated in other colours are the seventh, eighth and ninth layers added to generate larger model crystallites. Surface energies of the (100) and (010) planes were estimated in a similar fashion.

Scrolling simulations

Comparison of the crystal structures for **1a-c** reveals that lamellar hydrogen bonding networks are overwhelmingly favoured. In general, the gel fibres observed alongside crystals of structures **IX** and **X** are not crystalline, and there is no direct evidence that the molecules in these aggregates are packed in a lamellar fashion. However, surface energy calculations for a lamellar crystallite suggest that the growth in solution of expanded monolayer assemblies is highly feasible. Furthermore, gel formation is tentatively associated with crystalline lamellae displaying particular structural features, such as a lack of symmetry between the upper and lower surfaces. We hypothesise that both crystals and gels develop from lamellar assemblies in solution, and that gelation takes place when deformation of these structures results in a fibrous morphology. To identify the necessary conditions for fibre formation, it is useful to simulate the dynamics of multiple realistic lamellar configurations, which may conveniently be derived from single-crystal data. There is little justification, *a priori*, for assuming that crystalline lamellae are representative of those in solution. Nonetheless, this approach is remarkably successful in differentiating between systems that are weakly and strongly compatible with gel formation, and delivers a useful illustration of how unbranched, monodisperse fibrils might spontaneously arise.

For each crystal structure in this study, the folding behaviour of a single bis(urea) lamella was assessed by means of MD simulations. The model lamellae consisted of 600 molecules (Table S1) and were simulated in a vacuum at 300 K for 1500 ps, under the constant-*NVT* conditions previously discussed. The size and timeframe of the system were chosen to minimise computational cost: the simulations capture all major structural changes, and the lamellae are sufficiently large to avoid significant edge effects. Solvent was omitted in order to reduce the time for equilibration and assess how lamellae deform in response to internal stresses alone. Likewise, we did not attempt to replicate the non-isothermal conditions of a real gelation process,[54,68] since temperature changes may impact the system in different ways depending on the solvent, aggregate dimensions, gelator concentration and rate of cooling. Although the models do not account for effects such as viscosity, hydrophobicity and solvent-urea hydrogen bonding, the results illustrate the impact of key structural variables on lamellar morphology and provide a simple baseline for understanding the deformation pathways of more realistic, explicit-solvent simulations.

The bending modulus of a sheet scales roughly as the cube of its thickness τ.[97,98] Thus, it was expected that thinner lamellae would undergo folding more readily and attain larger curvatures at equilibrium. The value of τ cannot be gauged directly from the spacing of lamellae in a crystal, d_{layer}, as this distance is strongly influenced by interdigitation and the presence of solvent. A more reliable value may be arrived at by noting that bis(urea) molecules in the non-solvated structures **I**-**III** occupy a roughly constant volume V_{mol} = 620 ± 10 Å^3. Accordingly, τ may be equated to V_{mol}/A_{mol}, where A_{mol} is the area per molecule in the lamella. It is clear from the simulation results that this analysis offers only a weak indication of lamellar flexibility (Figure 11). For example, lamellae from structures **IV**, **VI** and **VIII**, display nearly identical values of τ, but produce starkly different outcomes in their folding simulations.

The simulations show that large, global curvatures occur only if the faces of the lamella are structurally dissimilar. Lamellae in structure **IX** display marked asymmetry between their upper and lower faces and undergo extensive folding when simulated, attaining an equilibrium radius of curvature of roughly 2 nm. Furthermore, if the lamella is sufficiently large,[99,100] the system exhibits scrolling behaviour, wherein the upper face of one part of the lamella is layered onto the lower face of a separate region. It is thought that this process resembles the dynamics of lamellae in solution, and is responsible for the formation of gel fibres alongside crystals of structure **IX**. Comparable scrolling has been observed in a number of materials comprising asymmetric lamellar structures, including asbestos chrysotile needles and crystalline polymers such as poly(ethylene), γ-poly(vinylidene fluoride) and Nylon 66.[101]

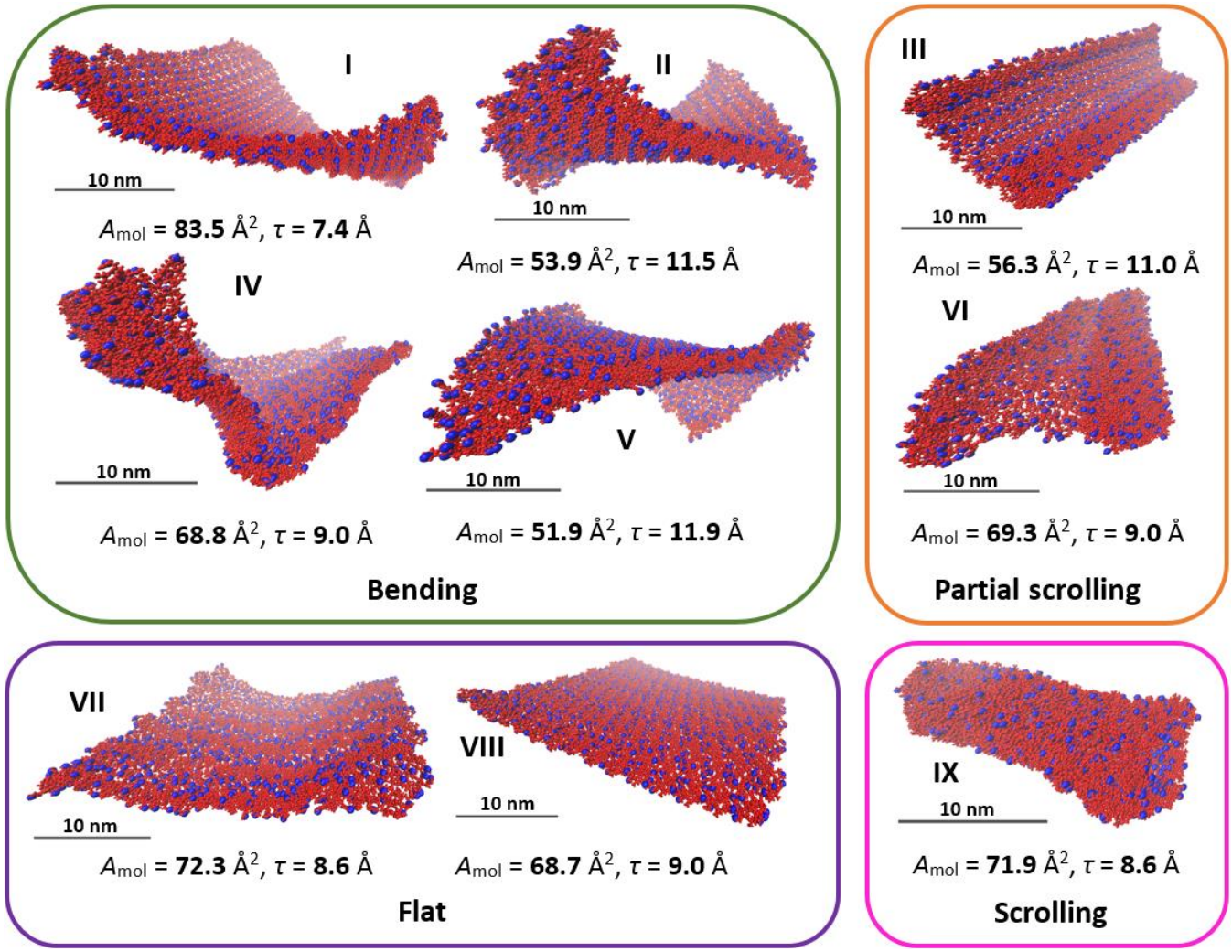

Figure 11 Final frames from 1500 ps MD simulations of lamellar bis(urea) networks from structures **I-IX**. Simulations were performed in a vacuum at 300 K, with the temperature controlled via a Berendsen thermostat. To highlight the end groups of the molecules, nitrogen atoms in the picolyl groups are shown as blue spheres with a 1.3 Å radius and all other atoms as red spheres with a 0.6 Å radius. Lamellae were constructed based on atomic positions calculated from the single-crystal X-ray structures and equilibrated via a steepest-descent procedure prior to the production run. The morphologies displayed for structures **III** and **VI** were obtained after equilibrating the model lamellae within four-layer crystallites at 300 K (see text). All images are representative of the lamellar morphology after equilibration, once all significant large-scale deformation has taken place. Values of A_{mol} were obtained from the single-crystal structures and τ was estimated as V_{mol}/A_{mol} with V_{mol} = 620 Å^3.

The outcome of scrolling is likely dependent on the geometric details of the lamella involved. As predicted by models of uniform sheets,[102] the time for equilibration scales with the dimensions of the system, as folding begins at the edges of lamella and produces only small displacements nearer the centre of the sheet. The rate of scrolling, meanwhile, is roughly constant at 10 nm ns^{-1} and does not vary significantly with the dimensions of the lamella (Figure S24). Unexpectedly, the axis of curvature is at 90° to the α-tape axis, and the face with the highest concentration of end groups forms the internal surface of the resulting fibril. The onset of scrolling, in which the lamella comes into contact with itself, is marked by a sharp decrease in potential energy and acceleration of folding (Figure 12). However, the process is not accompanied by any significant increase in hydrogen bonding (Figure S22b), suggesting that van der Waals forces and non-directional polar interactions are the major contributors to stabilisation. As observed in scrolling assemblies of amphiphilic copolymers, the decrease in energy exceeds the available thermal energy but is much less than the fusion energy of the system, so scrolling may proceed irreversibly without disrupting the hydrogen bonding network.[59]

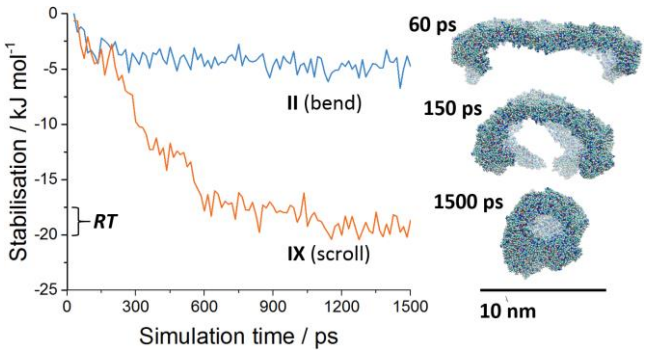

Figure 12 Changes in energy during MD simulations of lamellae with different modes of deformation, expressed per mole of bis(urea). Stabilisation energies are calculated relative to the maximum recorded energy values after 30 ps of simulation time, to allow the systems to equilibrate under constant-*NVT* conditions. Scrolling of a lamella from structure **IX** (right) begins at the edges of the system and is largely complete after 600 ps, producing a fibril roughly 7 nm in diameter.

Simulations of scrolling represent a simple and appealing model for the initial stages of fibril formation. Folding and growth of a lamella occur concurrently, so a fibril is likely to develop if the structure reaches an appreciable size before further layers are added. In nitrobenzene solutions of **1c**, it is proposed that scrolling and stacking of lamellae occur at similar rates, such that the competing processes of gelation and crystallisation are simultaneously observed. Comparable concomitant fibre growth alongside crystals of structure **X** at first seems surprising, as the bis(urea) molecules in this system are linked by a three-dimensional arrangement of hydrogen bonds. However, the bis(urea) network of structure **X** can be obtained by a continuous distortion of [AABB] lamellae, in which only one face is decorated with picolyl groups (Figure 13). MD simulations reveal that one such lamella can undergo spontaneous scrolling to form a fibril structure. As in the nitrobenzene system, the axis of curvature lies perpendicular to the α-tapes, and picolyl groups are located mostly on the inside of the fibril. We suggest that self-assembly in nitromethane initially generates [AABB] lamellae, which can either develop into fibrils or undergo stacking and recombination to form

a three-dimensional network. According to this model, the balance between gelation and crystallisation is determined by the relative rates of scrolling and stacking and may be highly solvent-dependent. For example, no concomitant gel is observed alongside the acetonitrile solvate **XI,** even though this structure and the nitromethane solvate **X** are isomorphous materials.

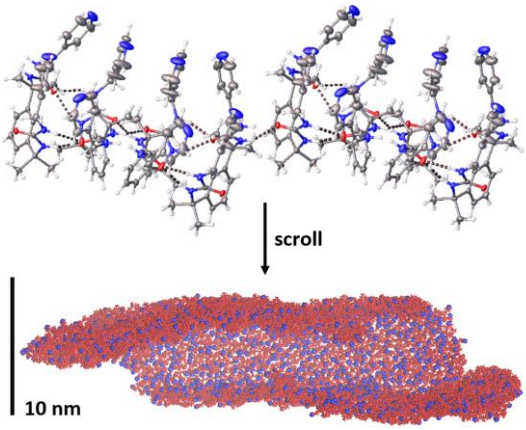

Figure 13 The three-dimensional network of α-tapes in structures **X** and **XI** can be divided into lamellae with an [AABB] repeat unit. Like those from structure **IX**, the lamellae are highly asymmetric and display scrolling behaviour in MD simulations.

Scrolling of lamellae is driven by an internal pressure resulting from structural asymmetry. The lack of gel formation in most of the systems studied may be linked to the abundance of crystal structures comprising symmetric lamellae. MD simulations confirm that lamellae with faces that are symmetry equivalent show no significant bias in their axis of curvature or folding direction. Indeed, even thin lamellae such as those of structure **I** tend to adopt crumpled or saddle-like morphologies,[63,64] and are thus deformed too little for scrolling behaviour to arise. Stabilisation due to folding is typically comparable to *RT* (Figure 12), and the incidence of multiple axes of curvature can further limit stabilisation. Crystallisation in such systems is the most favourable outcome, as there are no contacts between non-adjacent regions of the lamella to obstruct the growth of multilayer deposits.

It is worth emphasising that lamellar asymmetry, while necessary for scrolling, does not guarantee that such deformations will take place. Picolyl groups in structure **IV**, for example, are distributed unevenly between the two sides of the lamellar network, but lamellae are not sufficiently flexible for scrolling to arise. Conversely, MD simulations may predict scrolling due to asymmetric features that would not persist in the solution state. It was noted that lamellae from structures **III** and **VI** resemble those of structure **IX** in their folding behaviour, despite only small differences in molecular packing between their upper and lower faces (Figure S25). While folding of polymer sheets may result from differing arrangements of otherwise identical surface groups,[57] the geometric asymmetries in structures **III** and **VI** are induced largely by interactions with neighbouring lamellae, and are thus unlikely to emerge spontaneously before crystallisation takes place.

To test whether the asymmetries in structures **III** and **IV** could impact the dynamics of lamellae in solution, crystallites consisting of four lamellae in a vacuum were allowed to equilibrate for 300 ps at 300 K. This procedure enables the molecules to access a range of conformations, but constrains the overall lamellae to remain approximately planar. Subsequent simulations of each equilibrated lamella in isolation reveal more localised folding, with complete scrolling occurring in only a fraction of cases (Figure S25). By contrast, pre-equilibration of lamellae from structure **IX** does not affect their scrolling behaviour. The results suggest that a lamella in solution could not retain the geometric asymmetries of structures **III** and **VI**, and so would not be predisposed to significant scrolling. The polar distribution of picolyl groups in structure **IX**, however, represents a topological asymmetry, which cannot be removed without disassembling the lamellae. Given the mobility of molecules in solution, only topological asymmetries need be considered when assessing the likelihood of scrolling.

Schematic model

Scrolling of bis(urea) lamellae is analogous to the spontaneous curvature of micelle assemblies.[60] The two faces of a lamella occupy equal areas in the crystal structure but become more compact once neighbouring layers are removed. Interdigitation of lamellae in structure **IX**, for example, serves to fill the space between picolyl groups on the lamellar surface, so these groups must pack more closely when only one lamella is present (Figure 14). Bending occurs because one face of the lamella contracts more than the other, and is controlled by the sizes and packing efficiencies of the moieties involved. The axis of curvature is likely to lie parallel or perpendicular to the α-tapes since the groups either side of these axes are approximately symmetric. In addition, it is favourable for only one axis of curvature to exist, as bending about a second axis would cause stretching of the lamella and produce a high-energy dislocation where the axes intersect.[103] It is worth noting that folding in other systems may occur about an axis not parallel to one of the lamella edges. Such processes tends to produce a helical morphology,[97] but may ultimately give rise to hollow cylindrical fibrils if the pitch of the helix is less than or equal to the width of the lamella.[104]

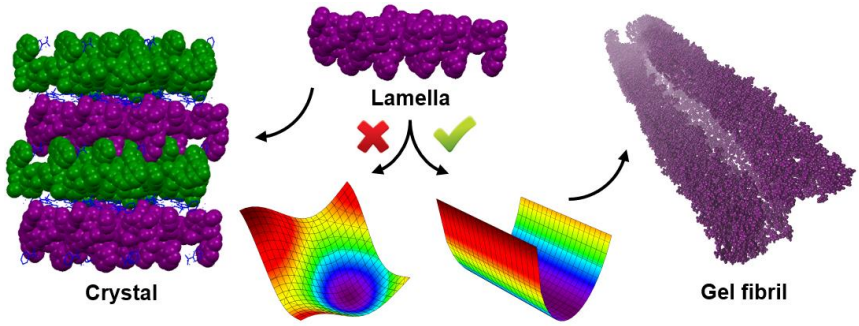

Figure 14 Lamellae in structure **IX** are arranged as symmetric bilayers. The faces of a single lamella, however, are asymmetric and must occupy different areas for optimal packing of the surface moieties. Thus, lamellae fold such that the face with the largest area is presented on the outer surface of the final structure. Cylindrical folding (centre right) can occur isotropically, as indicated by the uniform network of contour lines in the schematic illustration. By contrast, folding along two or more axes (centre left) leads to stretching of the surface and is energetically disfavoured. If the curvature is large enough, folding leads to scrolling of the lamella into a gel fibril (right), and prevents stacking to form a multilayer crystallite (left).

The direction of scrolling plays an important role in determining the physical properties of a gel fibril. Supramolecular motifs that are aligned with the fold axis may contribute more strongly to tensile strength,[105] and the moieties decorating the outer surface of the scrolled lamella are largely responsible for its adsorption behaviour.[106,107] Models of uniform lamellae show that the axis of curvature is determined by the relative lengths of the lamella edges.[102,108] However, real bis(urea) lamellae are not isotropic, and the simulations reveal that the favoured axis is that which offers the least resistance to bending deformations (Figure S23). Differences in the scrolling behaviour of lamellae from structures **III** and **VI** before and after equilibration (Figure S25) suggests that the geometry of scrolling is strongly influenced by molecular packing. Effects of this nature have been observed in supramolecular assemblies of rod-coil molecules, which adopt tubular morphologies only for particular combinations of in-plane bending moduli and respond sensitively to changes in molecular structure.[63,69]

The fibrils formed in MD simulations adopt realistic cylindrical, unbranched morphologies, but they are between two and four times narrower than the majority of fibrils observed in SEM images. Wider structures could arise through continued scrolling about the fibril circumference or accretion of additional layers to an existing fibril. It is worth noting that the equilibrium curvature of a scrolled lamella represents the most stable morphology, in which the intermolecular forces within and between the lamella are optimally balanced. Since increasing the fibril diameter reduces the curvature of the outer layer, each new layer is further from its energetic minimum. Thus, it is likely that lamellae beyond a critical radius will detach from the fibril to gain further stabilisation via scrolling (Figure 15a). This hypothesis is supported by SEM images of the materials, which reveal little variation in fibril

thickness (Figure 15b). Similar mechanisms have been proposed to explain the monodispersity of asbestos chrysotile needles[101] and, perhaps more strikingly, the inability of cylindrical objects to support climbing plants below a threshold helical radius (Figure 15c).[109] Indeed, such curvature-induced destabilisation is likely the dominant mechanism by which self-assembled aggregates attain well-defined morphologies.[110] For example, the dimensions of a helical fibre tend to be highly conserved because widening the structure leads to a rise in elastic strain, counterbalancing the favourable contribution of aggregate growth to the stability of the system.[111]

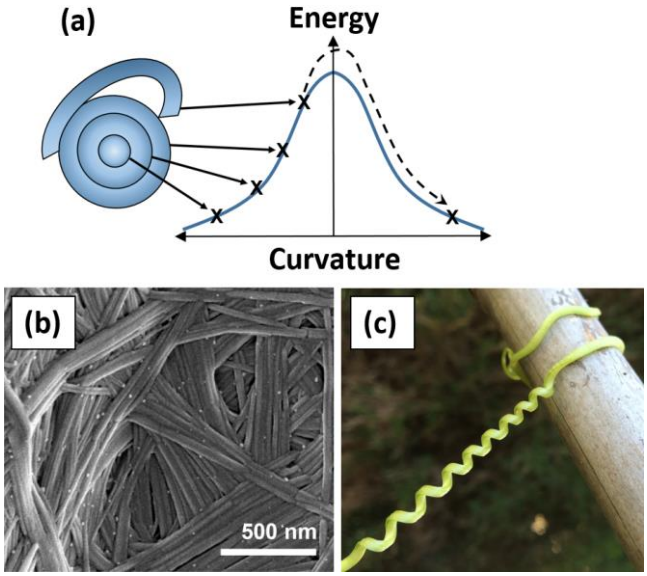

Figure 15 Schematic energy plot (a) for concentrically layered lamellae, illustrating how the decreasing local curvature with increasing radius leads to detachment of lamellae beyond a threshold fibre thickness. This phenomenon is potentially responsible for the uniformity of fibres in nitrobenzene gels of **1c** (b), and also underlies the inability of twining plants to wind several times around columns much larger than their helical diameter (c).

Given the simplicity and generality of the underlying physics, scrolling may represent an important step in the self-assembly of many LMWGs. Gelation due to scrolling is particularly probable if molecules are incorporated into asymmetric lamellae, with small bending moduli and limited interlayer hydrogen bonding. A tendency to self-assemble in this manner is most readily identified, as in this study, by combining MD simulations and microscopic observations with an extensive analysis of single-crystal structures. However, the feasibility of scrolling can likely be predicted even in the absence of crystallographic data. Lamellar aggregates can be detected via a range of experimental techniques, and may sometimes develop spontaneously in MD simulations.[67] Potential molecular arrangements may be extrapolated from studies of analogous compounds and ranked according to their stability in computational models.[68] Indeed, it may be even be possible, for molecules of limited flexibility, to generate an exhaustive catalogue of realistic crystal structures, allowing experimental observations to be matched to energetic minima in the self-assembly landscape.[112,113] Assessing the aggregation behaviour of a wider library of candidate LMWGs will lead to the identification of more general structure-property relationships, and provide a foundation for more detailed and predictive models of the gelation process.

Conclusions

Bis(urea)s are among the most popular examples of LMWGs, owing to their peptidomimetic characteristics and potent gelation capacities in a variety of organic solvents. The arrangement of hydrogen bonds in crystalline bis(urea)s is highly sensitive to both the solvent environment and end-group structure. Single-crystal diffraction studies have revealed that a series of picolyl-functionalised bis(urea)s form lamellar α-tape networks with a wide range of topologies. However, fibrous aggregates are observed only alongside crystals in which the bis(urea) lamellae are topologically asymmetric. The competition between two- and three-

dimensional self-assembly is decided largely by the relative surface energies of the crystal faces, which can be estimated through MD simulations of model assemblies. Crystallisation is favoured by factors that reduce this anisotropy, such as polar solvents that provide strong interlayer interactions and competitively bind to growing α-tapes. Gelation, meanwhile, occurs if multilayer aggregation is outpaced by the growth and folding of isolated monolayers. Atomistic simulations of single lamellae, based on the molecular arrangements of crystal structures, confirm that unbranched, monodisperse fibrils can develop from thin, asymmetric lamellae by spontaneous scrolling. Overall, this approach represents a simple, general and reliable method for predicting and analysing scrolling behavior in hydrogen bonded assemblies. The results offer useful insights into a crucial but underexplored stage of gel formation and could aid the identification of effective LMWGs from crystallographic data or predicted supramolecular assemblies.

ACCESSION NUMBERS

The accession numbers for the X-ray crystal structures reported in this paper are CCDC: 1547927, 1547930, 1548098, 1548101, 1548255, 1548256, 1548263, 1548264, 1548301, 1548302 and 1548307.

SUPPLEMENTAL INFORMATION

The Supplemental Information includes experimental details; spectroscopic data for compounds **1a-c**; photographs of selected gelation and crystallisation trials; rheometry data and SEM micrographs of gels; surface energy estimates from MD simulations of structure **II**; input structures and a sample topology file for simulations of bis(urea) lamellae; variations in temperature and hydrogen bond population during a typical simulation; final frames from simulated lamellae with differing dimensions, and after equilibration within a crystal lattice; and an analysis of bis(urea) structures in the CSD. Crystallographic Information Files (CIFs) for structures **I-XI** are also provided. Underlying research data is available from doi: 10.15128/r2tt44pm84v in accordance with the UK research councils' open data policy.

AUTHOR CONTRIBUTIONS

CDJ carried out all of the experimental work, MW and CDJ carried out the simulations, CDJ, SRK and DSY carried out the crystallography and CDJ and JWS wrote the paper. JWS supervised the project.

ACKNOWLEDGMENTS

This work was supported by the Engineering and Physical Sciences Research Council (EPSRC) via a Doctoral Scholarship (grant 1374655) and project grant EP/J013021/1, and by Diamond Light Source grant MT8682.

REFERENCES AND NOTES

1. Jones, C.D., and Steed, J.W. (2016). Gels with sense: supramolecular materials that respond to heat, light and sound. Chem. Soc. Rev. *45*, 6546-6596.
2. Díaz, D.D., Kühbeck, D., and Koopmans, R.J. (2011). Stimuli-responsive gels as reaction vessels and reusable catalysts. Chem. Soc. Rev. *40*, 427-448.
3. Moon, H.J., Ko, D.Y., Park, M.H., Joo, M.K., and Jeong, B. (2012). Temperature-responsive compounds as in situ gelling biomedical materials. Chem. Soc. Rev. *41*, 4860-4883.
4. Foster, J.A., Piepenbrock, M.O.M., Lloyd, G.O., Clarke, N., Howard, J.A.K., and Steed, J.W. (2010). Anion-switchable supramolecular gels for controlling pharmaceutical crystal growth. Nature Chem. *2*, 1037-1043.
5. Fitzpatrick, A.W.P., Debelouchina, G.T., Bayro, M.J., Clare, D.K., Caporini, M.A., Bajaj, V.S., Jaroniec, C.P., Wang, L.C., Ladizhansky, V., Müller, S.A., *et al.* (2013). Atomic structure and hierarchical assembly of a cross-beta amyloid fibril. Proc. Natl. Acad. Sci. U. S. A. *110*, 5468-5473.
6. Estroff, L.A., and Hamilton, A.D. (2004). Water gelation by small organic molecules. Chem. Rev. *104*, 1201-1217.
7. Adams, D.J., Morris, K., Chen, L., Serpell, L.C., Bacsa, J., and Day, G.M. (2010). The delicate balance between gelation and crystallisation: structural and computational investigations. Soft Matter *6*, 4144-4156.
8. Xu, H.Q., Song, J., Tian, T., and Feng, R.X. (2012). Estimation of organogel formation and influence of solvent viscosity and molecular size on gel properties and aggregate structures. Soft Matter *8*, 3478-3486.

9. Dastidar, P. (2008). Supramolecular gelling agents: can they be designed? Chem. Soc. Rev. *37*, 2699-2715.
10. Kumari, H., Armitage, S.E., Kline, S.R., Damodaran, K.K., Kennedy, S.R., Atwood, J.L., and Steed, J.W. (2015). Fluorous 'ponytails' lead to strong gelators showing thermally induced structure evolution. Soft Matter *11*, 8471-8478.
11. Kowalczuk, J., Bielejewski, M., Łapiński, A., Luboradzki, R., and Tritt-Goc, J. (2014). The Solvent–Gelator Interaction as the Origin of Different Diffusivity Behavior of Diols in Gels Formed with Sugar-Based Low-Molecular-Mass Gelator. J. Phys. Chem. B *118*, 4005-4015.
12. Rogers, M.A., Abraham, S., Bodondics, F., and Weiss, R.G. (2012). Influence of the Hydroxyl Position in Racemic Hydroxyoctadecanoic Acids on the Crystallization Kinetics and Activation Energies of Gels and Dispersions in Mineral Oil. Cryst. Growth Des. *12*, 5497-5504.
13. van Esch, J.H., and Feringa, B.L. (2000). New Functional Materials Based on Self-Assembling Organogels: From Serendipity towards Design. Angew. Chem. Int. Ed. *39*, 2263-2266.
14. Fuhrhop, J.H., Schnieder, P., Rosenberg, J., and Boekema, E. (1987). The chiral bilayer effect stabilizes micellar fibers. J. Am. Chem. Soc. *109*, 3387-3390.
15. Piepenbrock, M.O.M., Lloyd, G.O., Clarke, N., and Steed, J.W. (2008). Gelation is crucially dependent on functional group orientation and may be tuned by anion binding. Chem. Commun. *23*, 2644-2646.
16. Rogers, M.A., and Marangoni, A.G. (2009). Solvent-Modulated Nucleation and Crystallization Kinetics of 12-Hydroxystearic Acid: A Nonisothermal Approach. Langmuir *25*, 8556-8566.
17. Bajpai, A., Scott, H.S., Pham, T., Chen, K.J., Space, B., Lusi, M., Perry, M.L., and Zaworotko, M.J. (2016). Towards an understanding of the propensity for crystalline hydrate formation by molecular compounds. IUCrJ *3*, 430-439.
18. Vidyasagar, A., and Sureshan, K.M. (2015). Stoichiometric Sensing to Opt between Gelation and Crystallization. Angew. Chem. Int. Ed. *54*, 12078-12082.
19. Infantes, L., Fabian, L., and Motherwell, W.D.S. (2007). Organic crystal hydrates: what are the important factors for formation. Crystengcomm *9*, 65-71.
20. Desiraju, G.R. (1991). Hydration in organic-crystals - prediction from molecular-structure. J. Chem. Soc. Chem. Commun., 426-428.
21. Steed, K.M., and Steed, J.W. (2015). Packing Problems: High Z' Crystal Structures and Their Relationship to Cocrystals, Inclusion Compounds, and Polymorphism. Chem. Rev. *115*, 2895-2933.
22. Bardelang, D., Giorgi, M., Hornebecq, V., Stepanov, A., Rizzato, E., Zaman, M.B., Chan, G., Ouari, O., and Tordo, P. (2012). Perturbation induced formation of a 3D-network of microcrystals producing soft materials. RSC Adv. *2*, 5605-5609.
23. Li, G.H., Hu, Y.Y., Sui, J.F., Song, A.X., and Hao, J.C. (2016). Hydrogelation and Crystallization of Sodium Deoxycholate Controlled by Organic Acids. Langmuir *32*, 1502-1509.
24. Braga, D., d'Agostino, S., D'Amen, E., and Grepioni, F. (2011). Polymorphs from supramolecular gels: four crystal forms of the same silver(I) supergelator crystallized directly from its gels. Chem. Commun. *47*, 5154-5156.
25. Wang, Y.J., Tang, L.M., and Yu, J. (2008). Investigation of spontaneous transition from low-molecular-weight hydrogel into macroscopic crystals. Cryst. Growth Des. *8*, 884-889.
26. Martin, A.D., Wojciechowski, J.P., Bhadbhade, M.M., and Thordarson, P. (2016). A Capped Dipeptide Which Simultaneously Exhibits Gelation and Crystallization Behavior. Langmuir *32*, 2245-2250.
27. Cui, J.X., Shen, Z.H., and Wan, X.H. (2010). Study on the Gel to Crystal Transition of a Novel Sugar-Appended Gelator. Langmuir *26*, 97-103.
28. Anderson, K.M., Day, G.M., Paterson, M.J., Byrne, P., Clarke, N., and Steed, J.W. (2008). Structure calculation of an elastic hydrogel from sonication of rigid small molecule components. Angew. Chem. Int. Ed. *47*, 1058-1062.
29. Draper, E.R., Morris, K.L., Little, M.A., Raeburn, J., Colquhoun, C., Cross, E.R., McDonald, T.O., Serpell, L.C., and Adams, D.J. (2015). Hydrogels formed from Fmoc amino acids. Crystengcomm *17*, 8047-8057.
30. Houton, K.A., Morris, K.L., Chen, L., Schmidtmann, M., Jones, J.T.A., Serpell, L.C., Lloyd, G.O., and Adams, D.J. (2012). On Crystal versus Fiber Formation in Dipeptide Hydrogelator Systems. Langmuir *28*, 9797-9806.

31. Davey, R.J., Schroeder, S.L.M., and ter Horst, J.H. (2013). Nucleation of Organic Crystals—A Molecular Perspective. Angew. Chem. Int. Ed. *52*, 2166-2179.
32. Braun, D.E., Karamertzanis, P.G., and Price, S.L. (2011). Which, if any, hydrates will crystallise? Predicting hydrate formation of two dihydroxybenzoic acids. Chem. Commun. *47*, 5443-5445.
33. Wu, S., Gao, J., Emge, T.J., and Rogers, M.A. (2013). Influence of solvent on the supramolecular architectures in molecular gels. Soft Matter *9*, 5942-5950.
34. Xing, B.G., Yu, C.W., Chow, K.H., Ho, P.L., Fu, D.G., and Xu, B. (2002). Hydrophobic interaction and hydrogen bonding cooperatively confer a vancomycin hydrogel: A potential candidate for biomaterials. J. Am. Chem. Soc. *124*, 14846-14847.
35. Belenguer, A.M., Lampronti, G.I., Cruz-Cabeza, A.J., Hunter, C.A., and Sanders, J.K.M. (2016). Solvation and surface effects on polymorph stabilities at the nanoscale. Chem. Sci. *7*, 6617-6627.
36. Yoo, S.H., Eom, T., Kwon, S., Gong, J., Kim, J., Cho, S.J., Driver, R.W., Lee, Y., Kim, H., and Lee, H.S. (2015). Foldecture as a Core Material with Anisotropic Surface Characteristics. J. Am. Chem. Soc. *137*, 2159-2162.
37. Ozgur, B., and Sayar, M. (2016). Assembly of Triblock Amphiphilic Peptides into One-Dimensional Aggregates and Network Formation. J. Phys. Chem. B *120*, 10243-10257.
38. Sun, J.C., Zhang, H., Guo, K., and Yuan, S.L. (2015). Self-assembly of dipeptide sodium salts derived from alanine: a molecular dynamics study. Rsc Advances *5*, 102182-102190.
39. Eckes, K.M., Mu, X.J., Ruehle, M.A., Ren, P.Y., and Suggs, L.J. (2014). beta Sheets Not Required: Combined Experimental and Computational Studies of Self-Assembly and Gelation of the Ester-Containing Analogue of an Fmoc-Dipeptide Hydrogelator. Langmuir *30*, 5287-5296.
40. Ogata, K., Uchida, W., and Nakamura, S. (2014). Understanding Thermal Phases in Atomic Detail by All-Atom Molecular-Dynamics Simulation of a Phospholipid Bilayer. J. Phys. Chem. B *118*, 14353-14365.
41. Huang, M.J., Kapral, R., Mikhailov, A.S., and Chen, H.Y. (2012). Coarse-grain model for lipid bilayer self-assembly and dynamics: Multiparticle collision description of the solvent. J. Chem. Phys. *137*, 10.
42. Benner, S.W., and Hall, C.K. (2016). Development of a Coarse-Grained Model of Chitosan for Predicting Solution Behavior. J. Phys. Chem. B *120*, 7253-7264.
43. Luo, C.F., Kröger, M., and Sommer, J.U. (2016). Entanglements and Crystallization of Concentrated Polymer Solutions: Molecular Dynamics Simulations. Macromolecules *49*, 9017-9025.
44. Anderson, J.A., and Travesset, A. (2006). Coarse-grained simulations of gels of nonionic multiblock copolymers with hydrophobic groups. Macromolecules *39*, 5143-5151.
45. Srinivas, G., Discher, D.E., and Klein, M.L. (2004). Self-assembly and properties of diblock copolymers by coarse-grain molecular dynamics. Nature Mater. *3*, 638-644.
46. Rutkowski, D.M., Velev, O.D., Klapp, S.H.L., and Hall, C.K. (2016). The effect of charge separation on the phase behavior of dipolar colloidal rods. Soft Matter *12*, 4932-4943.
47. Horsch, M.A., Zhang, Z., and Glotzer, S.C. (2006). Self-assembly of laterally-tethered nanorods. Nano Lett. *6*, 2406-2413.
48. Grünwald, M., Tricard, S., Whitesides, G.M., and Geissler, P.L. (2016). Exploiting non-equilibrium phase separation for self-assembly. Soft Matter *12*, 1517-1524.
49. Perez, T., Liu, Y., Li, W., Gunton, J.D., and Chakrabarti, A. (2011). Pathways of Cluster Growth and Kinetic Slowing Down in a Model of Short-Range Attractive Colloids. Langmuir *27*, 11401-11408.
50. Marrink, S.J., Risselada, J., and Mark, A.E. (2005). Simulation of gel phase formation and melting in lipid bilayers using a coarse grained model. Chem. Phys. Lipids *135*, 223-244.
51. Stevens, M.J. (2004). Coarse-grained simulations of lipid bilayers. J. Chem. Phys. *121*, 11942-11948.
52. Chen, Y., Zhu, B., Zhang, F., Han, Y., and Bo, Z. (2008). Hierarchical Supramolecular Self-Assembly of Nanotubes and Layered Sheets. Angew. Chem. Int. Ed. *47*, 6015-6018.

53. Baburkin, P.O., Komarov, P.V., Khizhnyak, S.D., and Pakhomov, P.M. (2015). Simulation of gelation process in cysteine-silver solution by dissipative particle dynamics method. Colloid J. *77*, 561-570.
54. Verma, R.P., Shandilya, A., and Haridas, V. (2015). Peptide dendrimers with designer core for directed self-assembly. Tetrahedron *71*, 8758-8765.
55. Komarov, P.V., Mikhailov, I.V., Alekseev, V.G., Khizhnyak, S.D., and Pakhomov, P.M. (2011). Full-atom molecular dynamics study of structure and stability of filament-like aggregates formed by silver mercaptide molecules. Colloid J. *73*, 482-494.
56. Han, M., Hyun, J., and Sim, E. (2013). Formation of Rigid Organic Nanotubes with Controlled Internal Cavity Based on Frustrated Aggregate Internal Rearrangement Mechanism. J. Phys. Chem. B *117*, 7763-7770.
57. Han, M., and Sim, E. (2012). Surface Graft Configuration Dependency of the Morphologies of Heterosurface Sheet Polymers. J. Phys. Chem. B *116*, 5771-5776.
58. Han, M., and Sim, E. (2012). Formation of Tubular Scrolls with Controlled Internal Cavity. J. Phys. Chem. B *116*, 1796-1801.
59. Xiong, H.M., Chen, C.K., Lee, K., Van Horn, R.M., Liu, Z., Ren, B., Quirk, R.P., Thomas, E.L., Lotz, B., Ho, R.M., *et al.* (2011). Scrolled Polymer Single Crystals Driven by Unbalanced Surface Stresses: Rational Design and Experimental Evidence. Macromolecules *44*, 7758-7766.
60. Israelachvili, J.N., Mitchell, D.J., and Ninham, B.W. (1976). Theory of self-assembly of hydrocarbon amphiphiles into micelles and bilayers. J. Chem. Soc., Faraday Trans. II *72*, 1525-1568.
61. Zanuy, D., Poater, J., Solà, M., Hamley, I.W., and Alemán, C. (2016). Fmoc-RGDS based fibrils: atomistic details of their hierarchical assembly. Phys. Chem. Chem. Phys. *18*, 1265-1278.
62. Knauert, S.T., Douglas, J.F., and Starr, F.W. (2010). Morphology and Transport Properties of Two-Dimensional Sheet Polymers. Macromolecules *43*, 3438-3445.
63. Bowick, M., Falcioni, M., and Thorleifsson, G. (1997). Numerical observation of a tubular phase in anisotropic membranes. Phys. Rev. Lett. *79*, 885-888.
64. Radzihovsky, L., and Toner, J. (1995). A new phase of tethered membranes: Tubules. Phys. Rev. Lett. *75*, 4752-4755.
65. Groot, R.D., and Warren, P.B. (1997). Dissipative particle dynamics: Bridging the gap between atomistic and mesoscopic simulation. J. Chem. Phys. *107*, 4423-4435.
66. Sasselli, I.R., Pappas, C.G., Matthews, E., Wang, T., Hunt, N.T., Ulijn, R.V., and Tuttle, T. (2016). Using experimental and computational energy equilibration to understand hierarchical self-assembly of Fmoc-dipeptide amphiphiles. Soft Matter *12*, 8307-8315.
67. Sun, Y.X., Qian, Z.Y., Guo, C., and Wei, G.H. (2015). Amphiphilic Peptides A(6)K and V6K Display Distinct Oligomeric Structures and Self-Assembly Dynamics: A Combined All-Atom and Coarse-Grained Simulation Study. Biomacromolecules *16*, 2940-2949.
68. Mu, X.J., Eckes, K.M., Nguyen, M.M., Suggs, L.J., and Ren, P.Y. (2012). Experimental and Computational Studies Reveal an Alternative Supramolecular Structure for Fmoc-Dipeptide Self-Assembly. Biomacromolecules *13*, 3562-3571.
69. Hong, D.J., Lee, E., Jeong, H., Lee, J., Zin, W.C., Nguyen, T.D., Glotzer, S.C., and Lee, M. (2009). Solid-State Scrolls from Hierarchical Self-Assembly of T-Shaped Rod-Coil Molecules. Angew. Chem. Int. Ed. *48*, 1664-1668.
70. van Esch, J., De Feyter, S., Kellogg, R.M., De Schryver, F., and Feringa, B.L. (1997). Self-Assembly of Bisurea Compounds in Organic Solvents and on Solid Substrates. Chem. Eur. J. *3*, 1238-1243.
71. Kumari, H., Kline, S.R., Kennedy, S.R., Garvey, C., Raston, C.L., Atwood, J.L., and Steed, J.W. (2016). Manipulating three-dimensional gel network entanglement by thin film shearing. Chem. Commun. *52*, 4513-4516.
72. Schoonbeek, F.S., van Esch, J.H., Wegewijs, B., Rep, D.B.A., de Haas, M.P., Klapwijk, T.M., Kellogg, R.M., and Feringa, B.L. (1999). Efficient intermolecular charge transport in self-assembled fibers of mono- and bithiophene bisurea compounds. Angew. Chem. Int. Ed. *38*, 1393-1397.
73. Gesquière, A., De Feyter, S., Schoonbeek, F., van Esch, J., Kellogg, R.M., and Feringa, B.L. (2001). Supramolecular π-Stacked Assemblies of Bis(urea)-Substituted Thiophene Derivatives and Their Electronic Properties Probed with Scanning Tunneling Microscopy and Scanning Tunneling Spectroscopy. Nano Lett. *1*, 201-206.

74. Smith, A.M., Williams, R.J., Tang, C., Coppo, P., Collins, R.F., Turner, M.L., Saiani, A., and Ulijn, R.V. (2008). Fmoc-Diphenylalanine Self Assembles to a Hydrogel via a Novel Architecture Based on π–π Interlocked β-Sheets. Adv. Mater. *20*, 37-41.
75. Zhao, X.Q., Chang, Y.L., Fowler, F.W., and Lauher, J.W. (1990). An approach to the design of molecular-solids - the ureylenedicarboxylic acids. J. Am. Chem. Soc. *112*, 6627-6634.
76. Steed, J.W. (2010). Anion-tuned supramolecular gels: a natural evolution from urea supramolecular chemistry. Chem. Soc. Rev. *39*, 3686-3699.
77. Byrne, P., Turner, D.R., Lloyd, G.O., Clarke, N., and Steed, J.W. (2008). Gradual transition from NH center dot center dot center dot pyridyl hydrogen bonding to the NH center dot center dot center dot O tape synthon in pyridyl ureas. Cryst. Growth Des. *8*, 3335-3344.
78. Custelcean, R. (2008). Crystal engineering with urea and thiourea hydrogen-bonding groups. Chem. Commun., 295-307.
79. Reddy, L.S., Chandran, S.K., George, S., Babu, N.J., and Nangia, A. (2007). Crystal Structures of N-Aryl-N′ -4-Nitrophenyl Ureas: Molecular Conformation and Weak Interactions Direct the Strong Hydrogen Bond Synthon. Cryst. Growth Des. *7*, 2675-2690.
80. Cayuela, A., Kennedy, S.R., Soriano, M.L., Jones, C.D., Valcárcel, M., and Steed, J.W. (2015). Fluorescent carbon dot-molecular salt hydrogels. Chem. Sci. *6*, 6139-6146.
81. Meazza, L., Foster, J.A., Fucke, K., Metrangolo, P., Resnati, G., and Steed, J.W. (2013). Halogen-bonding-triggered supramolecular gel formation. Nature Chem. *5*, 42-47.
82. Piepenbrock, M.O.M., Clarke, N., and Steed, J.W. (2010). Shear induced gelation in a copper(II) metallogel: new aspects of ion-tunable rheology and gel-reformation by external chemical stimuli. Soft Matter *6*, 3541-3547.
83. Todd, A.M., Anderson, K.M., Byrne, P., Goeta, A.E., and Steed, J.W. (2006). Helical or Polar Guest-Dependent Z′ = 1.5 or Z′ = 2 Forms of a Sterically Hindered Bis(urea) Clathrate. Cryst. Growth Des. *6*, 1750-1752.
84. Groom, C.R., Bruno, I.J., Lightfoot, M.P., and Ward, S.C. (2016). The Cambridge Structural Database. Acta Crystallographica Section B-Structural Science Crystal Engineering and Materials *72*, 171-179.
85. Brocorens, P., Linares, M., Guyard-Duhayon, C., Guillot, R., Andrioletti, B., Suhr, D., Isare, B., Lazzaroni, R., and Bouteiller, L. (2013). Conformational Plasticity of Hydrogen Bonded Bis-urea Supramolecular Polymers. J. Phys. Chem. B *117*, 5379-5386.
86. Bernstein, J., Davis, R.E., Shimoni, L., and Chang, N.L. (1995). Patterns in hydrogen bonding - functionality and graph set analysis in crystals. Angew. Chem. Int. Ed. *34*, 1555-1573.
87. Geer, M.F., Smith, M.D., and Shimizu, L.S. (2011). A bis-urea naphthalene macrocycle displaying two crystal structures with parallel ureas. CrystEngComm *13*, 3665-3669.
88. Groom, C.R., Bruno, I.J., Lightfoot, M.P., and Ward, S.C. (2016). The Cambridge Structural Database. Acta Crystallogr. Sect. B *72*, 171-179.
89. Fucke, K., McIntyre, G.J., Lemée-Cailleau, M.H., Wilkinson, C., Edwards, A.J., Howard, J.A.K., and Steed, J.W. (2015). Insights into the Crystallisation Process from Anhydrous, Hydrated and Solvated Crystal Forms of Diatrizoic Acid. Chem. Eur. J. *21*, 1036-1047.
90. Thirunahari, S., Aitipamula, S., Chow, P.S., and Tan, R.B.H. (2010). Conformational polymorphism of tolbutamide: A structural, spectroscopic, and thermodynamic characterization of Burger's forms I–IV. J. Pharm. Sci. *99*, 2975-2990.
91. Terech, P., Pasquier, D., Bordas, V., and Rossat, C. (2000). Rheological properties and structural correlations in molecular organogels. Langmuir *16*, 4485-4494.
92. Yuan, B., Liu, X.Y., Li, J.L., and Xu, H.Y. (2011). Volume confinement induced microstructural transitions and property enhancements of supramolecular soft materials. Soft Matter *7*, 1708-1713.
93. Van der Spoel, D., Lindahl, E., Hess, B., Groenhof, G., Mark, A.E., and Berendsen, H.J.C. (2005). GROMACS: Fast, flexible, and free. J. Comput. Chem. *26*, 1701-1718.
94. Case, D.A., Cheatham, T.E., Darden, T., Gohlke, H., Luo, R., Merz, K.M., Onufriev, A., Simmerling, C., Wang, B., and Woods, R.J. (2005). The Amber biomolecular simulation programs. J. Computat. Chem. *26*, 1668-1688.

95. Wang, J.M., Wang, W., Kollman, P.A., and Case, D.A. (2006). Automatic atom type and bond type perception in molecular mechanical calculations. J. Mol. Graphics Modell. *25*, 247-260.
96. Berendsen, H.J.C., Postma, J.P.M., Vangunsteren, W.F., DiNola, A., and Haak, J.R. (1984). Molecular-dynamics with coupling to an external bath. J. Chem. Phys. *81*, 3684-3690.
97. Armon, S., Aharoni, H., Moshe, M., and Sharon, E. (2014). Shape selection in chiral ribbons: from seed pods to supramolecular assemblies. Soft Matter *10*, 2733-2740.
98. Birshtein, T.M., Lakovlev, P.A., Arnoskov, V.M., Leermakers, F.A.M., Zhulina, E.B., and Borisov, O.V. (2008). On the curvature energy of a thin membrane decorated by polymer brushes. Macromolecules *41*, 478-488.
99. Bae, J., Ouchi, T., and Hayward, R.C. (2015). Measuring the Elastic Modulus of Thin Polymer Sheets by Elastocapillary Bending. ACS Appl. Mater. Interfaces *7*, 14734-14742.
100. Evans, A.A., Spagnolie, S.E., Bartolo, D., and Lauga, E. (2013). Elastocapillary self-folding: buckling, wrinkling, and collapse of floating filaments. Soft Matter *9*, 1711-1720.
101. Lotz, B., and Cheng, S.Z.D. (2005). A critical assessment of unbalanced surface stresses as the mechanical origin of twisting and scrolling of polymer crystals. Polymer *46*, 577-610.
102. Stoychev, G., Zakharchenko, S., Turcaud, S., Dunlop, J.W.C., and Ionov, L. (2012). Shape-Programmed Folding of Stimuli-Responsive Polymer Bilayers. ACS Nano *6*, 3925-3934.
103. Cerda, E., Chaieb, S., Melo, F., and Mahadevan, L. (1999). Conical dislocations in crumpling. Nature *401*, 46-49.
104. Jung, J.H., Lee, S.H., Yoo, J.S., Yoshida, K., Shimizu, T., and Shinkai, S. (2003). Creation of double silica nanotubes by using crown-appended cholesterol nanotubes. Chem. Eur. J. *9*, 5307-5313.
105. Paavilainen, S., McWhirter, J.L., Rog, T., Jarvinen, J., Vattulainen, I., and Ketoja, J.A. (2012). Mechanical properties of cellulose nanofibrils determined through atomistic molecular dynamics simulations. Nord. Pulp Paper Res. J. *27*, 282-286.
106. Liu, K.Y., Meng, L.Y., Mo, S.L., Zhang, M.M., Mao, Y.Y., Cao, X.H., Huang, C.H., and Yi, T. (2013). Colour change and luminescence enhancement in a cholesterol-based terpyridyl platinum metallogel via sonication. J. Mater. Chem. C *1*, 1753-1762.
107. Wu, J.C., Yi, T., Shu, T.M., Yu, M.X., Zhou, Z.G., Xu, M., Zhou, Y.F., Zhang, H.J., Han, J.T., Li, F.Y., *et al.* (2008). Ultrasound switch and thermal self-repair of morphology and surface wettability in a cholesterol-based self-assembly system. Angew. Chem. Int. Ed. *47*, 1063-1067.
108. Alben, S., Balakrisnan, B., and Smela, E. (2011). Edge Effects Determine the Direction of Bilayer Bending. Nano Lett. *11*, 2280-2285.
109. Goriely, A., and Neukirch, S. (2006). Mechanics of climbing and attachment in twining plants. Phys. Rev. Lett. *97*, 184302.
110. Yashima, E., Ousaka, N., Taura, D., Shimomura, K., Ikai, T., and Maeda, K. (2016). Supramolecular Helical Systems: Helical Assemblies of Small Molecules, Foldamers, and Polymers with Chiral Amplification and Their Functions. Chem. Rev. *116*, 13752-13990.
111. Aggeli, A., Nyrkova, I.A., Bell, M., Harding, R., Carrick, L., McLeish, T.C.B., Semenov, A.N., and Boden, N. (2001). Hierarchical self-assembly of chiral rod-like molecules as a model for peptide beta-sheet tapes, ribbons, fibrils, and fibers. Proc. Natl. Acad. Sci. U. S. A. *98*, 11857-11862.
112. Foster, J.A., Damodaran, K.K., Maurin, A., Day, G.M., Thompson, H.P.G., Cameron, G.J., Bernal, J.C., and Steed, J.W. (2017). Pharmaceutical polymorph control in a drug-mimetic supramolecular gel. Chem. Sci. *8*, 78-84.
113. Piana, F., Case, D.H., Ramalhete, S.M., Pileio, G., Facciotti, M., Day, G.M., Khimyak, Y.Z., Angulo, J., Brown, R.C.D., and Gale, P.A. (2016). Substituent interference on supramolecular assembly in urea gelators: synthesis, structure prediction and NMR. Soft Matter *12*, 4034-4043.